# The Effect of Processing Parameters on Ferromanganese Alloy Carbon Content in Mamatwan Ore Reduction

Theresa Coetsee

e-mail: theresa.coetsee@up.ac.za

Department of Materials Science and Metallurgical Engineering, University of Pretoria, South Africa

## Abstract

Industrial production of medium carbon ferromanganese is accomplished by decarburisation of high carbon ferromanganese in an oxygen blown converter. In this study the possible in situ refinement of high carbon ferromanganese was tested in carbon deficient mixtures of pre-reduced Mamatwan ore, coal char and silica flux reacted at furnace temperatures of 1450°-1550°C. The resultant phase chemistry was analysed and interpreted with the aid of thermochemical calculations. Production of carbon unsaturated ferromanganese alloy in the AlloyStream process is explained with reference to laboratory experimental results.

Keywords:  reduction; manganese; mineralogy; basicity

## 1. Introduction

Medium carbon ferromanganese (MCFeMn) is produced by decarburisation of high carbon ferromanganese (HCFeMn) in an oxygen blown converter. This process requires high temperatures up to 1750°C and vigorous mixing to drive process kinetics. One of the disadvantages is high losses of manganese to slag an off gas, reaction products which must be recycled to the high carbon ferromanganese furnace to improve overall manganese recovery levels (Habashi, 1997). If the ferromanganese alloy carbon level could be managed to lower levels already in the primary production process of HCFeMn, the need for the current high intensity, low manganese recovery converter process step may be negated.

Terayama and Ikeda (1985) reacted pure MnO and C at the mole ratio of one (mol C/mol MnO = 1/1) at 1200°C and concluded, from XRD (X-ray diffraction) analyses of the reaction product, that the initially formed $Mn_7C_3$ was converted to Mn metal at complete reaction extent. When the carbon addition was increased to a mole ratio of 2.5, the product was $Mn_7C_3$, indicating that no conversion to Mn took place. The conclusion was that conversion of $Mn_7C_3$ took place according to reaction (1). From FactSage 6.4 thermochemical calculations, reaction (1) occurs at temperatures above 938°C.

$$Mn_7C_3 + 3CO_2 = 7Mn + 6CO \tag{1}$$

The AlloyStream process was originally developed to produce steel directly from mixed feed of iron ore, coal and fluxes, as described in U.S. patent 6146437 (Fourie, 2000). Therefore, the process provided conditions of higher oxygen potential in contact with the alloy to ensure minimal dissolution of carbon from coal into the alloy phase so that steel was produced and not cast iron. The process consisted of feeding -10 mm raw material mixture through the furnace combustion zone (freeboard) onto a liquid alloy bath, forming heaps of reacted material; the heap material is heated at the heap top surface by heat generated from burning combustibles with oxygen enriched air in the freeboard. The combustibles consist of fuel gas, coal volatiles, coal carbon and reduction reaction product gas emanating from the heaps. Final reaction and smelting of the heap material is supported by energy transferred from the induction-heated alloy bath.

The results of Terayama and Ikeda (1985) on MnO reduction and direct production of steel in the AlloyStream process led to the main objective of this work to test if medium carbon ferromanganese alloy may be produced by reaction of manganese ore at carbon deficient levels (mol C/mol MnO <1), and investigate the attainable levels of manganese recovery to the alloy. In addition, the effect of reduction parameters was tested in terms of level of carbon addition, reaction temperature and reaction time.

The presence of gangue oxides and iron oxides in manganese ores results in a reaction set-up which is expected to be more complex than that used in the study by Terayama and Ikeda (1985). Mamatwan ore is used extensively in the local ferromanganese production industry. Mamatwan ore reduction follows a sequence of two to three distinctive reduction stages (Koursaris et al., 1983; Koursaris and See, 1979; Eric and Burucu, 1992). In the rapid first stage CO reduction of higher oxides of manganese and iron to MnO and FeO occurs. In the markedly slower second stage of reduction metallisation of FeO and MnO starts. Metallisation begins with metallic iron nucleation throughout the reduced ore particle, adjacent to solid monoxide particles within the liquid silicate slag (provided the temperature is high enough to form liquid slag). As manganese reduction progresses the iron nuclei are alloyed with manganese and carbon. In the third stage final reduction of MnO by carbon dissolved in the alloy phase occurs at the solid monoxide-alloy phase interface. The third stage has the lowest reduction rate, most likely due to the slow diffusion of $Mn^{2+}$ ions in the monoxide phase, and/or liquid slag phase coating the monoxide phase (Eric and Burucu, 1992).

Once the alloy beads and manganese monoxide phase areas are encapsulated in the liquid silicate phase inside the reduced ore particle, reduction by CO gas is hindered, and reduction may proceed at the ore particle surface by solid carbon and carbon in alloy, and/or inside the reduced ore particle by carbon in alloy particles.

The Mamatwan ore used in this work contained braunite ($MnO.3Mn_2O_3.SiO_2$) as the main mineral, and minor minerals of carbonate type, kutnohorite ($Ca(Mn,Mg)(CO_3)_2$) and calcite($CaCO_3$). The ore was pre-reduced to MnO and FeO to simplify the ore mineralogy and to eliminate the possible interference of $CO_2$ gas from ore carbonate calcination in the reduction experiments. In the industrial production of high carbon ferromanganese the discard slag practise is applied to ensure maximum manganese recovery to the alloy from basic ores such as Mamatwan ore (Habashi, 1997). Therefore, input mixtures in this study were selected to form high basicity slag in accordance with the discard slag practice.


## 2. Experimental

### 2.1. Raw materials

Mixtures of pre-reduced Mamatwan ore (-6.3 mm), Eikeboom char (-2 mm) and silica flux (-1 mm) were reacted at temperatures of 1450°C, 1500°C and 1550°C. Analyses of pre-reduced Mamatwan ore and Eikeboom char are presented in Table 1 and Table 2. Chemical analyses of Mamatwan ore, char ash and silica flux were done by Inductively Coupled Plasma Optical Emission Spectrometry (ICP-OES) method. Bulk product metal carbon analyses and char ultimate analysis (C, H, N) were done by combustion (LECO) analysis method.

Eikeboom coal was devolatilised at 1000°C under $N_2$ atmosphere. Mamatwan ore was pre-reduced to MnO and FeO by reduction at 1000°C under CO atmosphere. The carbonates present in the Mamatwan ore was nearly fully calcinated, as indicated by low level for carbon analysed in the pre-reduced ore, expressed as $CaCO_3$ in Table 1. The level of pre-reduction is confirmed by the total of the pre-reduced ore chemical analysis of 99 mass% for the compounds as in Table 1.

Char addition in each mixture was calculated by mass balance for the target level of manganese metallisation from MnO, 100% iron metallisation from FeO in the ore and $Fe_2O_3$ in the char ash and flux, and 2%C in the expected alloy mass, assuming the reduction reaction product gas consisted of CO only, and the only $CO_2$ in

the product gas was generated by calcination of the small quantities of $CaCO_3$ and $MgCO_3$ present in the silica flux (99 mass% $SiO_2$). The level of char addition was expressed as the mol ratio of carbon to reducible oxygen (C/O) to meaningfully present the importance of carbon addition, as compared to a mass% carbon addition number. In the (C/O) value, reducible oxygen (O) is the sum of the oxygen associated with Mn and Fe oxides, and C is the value from the ultimate analysis in Table 2. Silica flux additions were made to attain the aim slag basicity of (%CaO/%$SiO_2$)=B2=1.04 and (%CaO +%MgO)/%$SiO_2$=B3=1.34, estimated to be sufficient for MgO saturation at 1500°C at 80% manganese recovery to the alloy. A summary of the experimental conditions is contained in Table 3.

**Table 1: Mamatwan pre-reduced ore bulk chemical composition**

|  | Mass% |
|---|---|
| MnO | 62.37 |
| FeO | 7.58 |
| $SiO_2$ | 7.73 |
| $Al_2O_3$ | 0.29 |
| CaO | 15.90 |
| MgO | 4.59 |
| $TiO_2$ | 0.04 |
| K2O | 0.03 |
| $CaCO_3$ | 0.50 |
| S | 0.05 |
| Total | 99.08 |

**Table 2: Eikeboom char bulk composition (mass percentages)**

| Proximate analysis (dry basis) | |
|---|---|
| Moisture | 0.1 |
| Volatile matter | 0.4 |
| Fixed carbon | 82.7 |
| Ash | 16.9 |
| Ultimate analysis (dry basis) | |
| C | 79.8 |
| H | 0.35 |
| N | 1.11 |
| O | 1.48 |
| S | 0.36 |
| Ash analysis (dry basis) | |
| $SiO_2$ | 54.50 |
| $Al_2O_3$ | 36.10 |
| $Fe_2O_3$ | 3.76 |
| $TiO_2$ | 2.00 |
| CaO | 1.53 |
| MgO | 0.41 |
| MnO | 0.03 |
| $Na_2O$ | 0.09 |
| $K_2O$ | 0.56 |
| $P_2O_5$ | 0.62 |
| $Cr_2O_3$ | 0.23 |
| S | 0.09 |

**Table 3: Feed material mixtures and furnace temperatures**

| Sample Name | mass% pre-reduced ore | mass% Char | mass% Silica | C/O | Aim %Mn recovery | *Furnace Temperature (°C) |
|---|---|---|---|---|---|---|
| A | 84.2 | 10.1 | 5.7 | 0.79 | 70 | 1500 |
| B | 82.8 | 11.8 | 5.5 | 0.94 | 85 | 1500 |
| C | 81.4 | 13.4 | 5.2 | 1.08 | 100 | 1500 |
| D | 82.8 | 11.8 | 5.5 | 0.94 | 85 | 1450 |
| E | 82.8 | 11.8 | 5.5 | 0.94 | 85 | 1550 |
| F | 82.8 | 11.8 | 5.5 | 0.94 | 85 | 1550 |
| G | 82.8 | 11.8 | 5.5 | 0.94 | 85 | 1550 |

*Furnace hot zone temperature

## 2.2. Experimental set-up

The sample mixture mass was ± 50 gram, with 42.2 gram of pre-reduced ore as basis. The sample mixture was contained in an MgO crucible and introduced under Ar into the hot zone of the tube furnace, via the pedestal. The MgO crucible was held in an alumina safety crucible to protect the furnace tube in case of MgO crucible failure. After the requisite reaction period passed, the sample was lowered into a cooling box, and the slide gate separating the furnace tube and cooling box was closed. The sample was cooled under Ar. The cooled sample was set in epoxy to form a polished section, which was then halved. From one half polished section, the alloy was separated out for bulk analyses for %Mn, %Fe and %C. The other half of the polished section was analysed by SEM (Scanning electron microscopy) using wavelength-dispersive X-ray spectrometry (WDX) to characterise the sample phase chemistry.

Throughout the experiment, the product gas was analysed by mass spectrometer for Ar, CO and $CO_2$. The Argon carrier gas flow rate was measured before each experiment by using a soap bubble meter, and flow rate control was done by rotameter fed from an Ar bottle via a pressure regulator. Argon gas of 99.999% purity was used as carrier gas at a flow rate of 1028 $cm^3$/min. The Ar gas was cleaned by passing through anhydrous $CaSO_4$ to remove water ("Drierite"), and through an "Oxyzorb" cartridge to remove oxygen. From the water cooled top lid of the furnace, the product gas passed through a filter to remove any dust particles present in the gas stream. The product gas flowed past a draw off point from which a continuous sample stream was drawn off to the mass spectrometer (VG Gaslab 300) for analyses, and the product gas then flowed through a bubbler to the vent. The mass spectrometer was calibrated prior to each set of experiments. The calibration gases used were 100%CO, 100%Ar and 10%$CO_2$-Ar, respectively.

## 3. Results and discussion

## 3.1. Product analyses and features

The product gas consisted mainly of CO, as very little $CO_2$ was measured in the product gas analyses. Samples A to E were reacted until the CO concentration in the product gas dissipated to zero percent. The product gas analyses data for sample E is plotted in Figure 1. Due to the presence of both manganese and iron oxides in the feed mixture, it is not possible to allocate the CO quantities measured to a specific reduction reaction. The total oxygen content in the product gas does allow for monitoring the reaction extent over time in each experiment so that the relative performance under different reaction conditions may be compared. This information is plotted in Fig. 2 with percentage reduction expressed as the mass of oxygen in CO and $CO_2$ in the product gas, as a percentage of the reducible oxygen in the feed mixture. A time marker is superimposed onto each curve, indicating the time taken to lift the sample to the furnace hot zone target position. This

period of time was 35-40 minutes, at a lifting rate of typically 2 cm/minute. It is seen that sample A was lifted at a somewhat slower rate of 1.5 cm/minute. Reaction time information is summarised in Table 4. Analyses of the bulk alloy recovered from one half of the polished section are summarised in Table 5. For samples F and G the quantity of coalesced alloy was insufficient to conduct bulk chemical analyses. The alloy compositions of samples A to E contain high levels of manganese and carbon, confirming that HCFeMn was formed as product alloy, despite the variation in C/O in the feed mixtures. Therefore, the bulk alloy analyses confirmed that no bulk refinement of alloy carbon occurred at the experimental conditions used.

**Figure 1: Product gas analyses data for sample E**
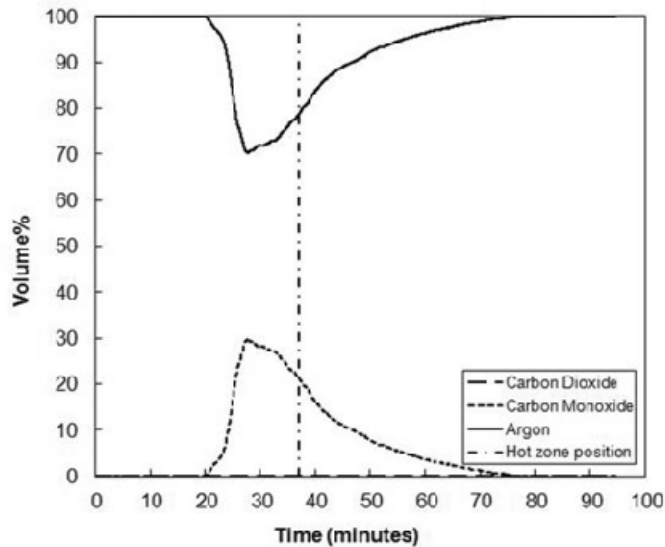


**Figure 2: Percentage reduction vs. time**
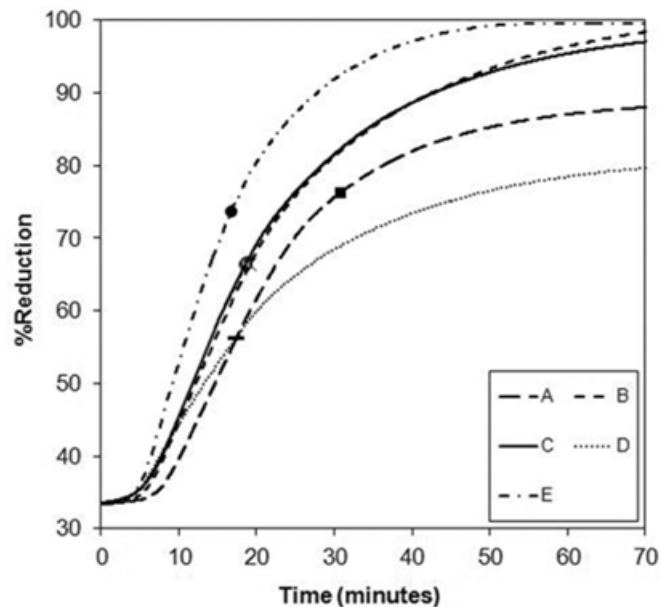


For samples A to E, the maximum CO concentration was measured before the sample reached the hot zone position as illustrated for sample E in Figure 1. To further investigate this initial period of reaction, a sample

was reacted for 40 minutes only (sample G, Table 4). This sample polished section may be compared to polished sections of samples A to E, indicating that significant reduction of MnO and FeO to alloy occurred early on at lower temperatures in sample G. However, final reduction to high recovery levels to the alloy and bulk separation of slag and alloy did not occur, as in the case of samples A to E. These observations are clear from comparison of the relative size and coalescence of alloy in the polished section photographs in Figure 3 (a-f), illustrating the complex interaction of melting and reduction in manganese ore. Therefore, detailed investigation of reduction in manganese ores should include the study of morphological changes in the ore due to phase chemistry changes as reduction proceeds, to enable interpretation of reduction progress over time. These mineralogical details are discussed in the following section. Comparison of percentage reduction graphs in Figure 2 illustrates the dominant effect of temperature increase from 1450°C to 1550°C on the reduction rate (graphs for samples D, B and E). The effect of carbon addition was only observed at the lowest level of carbon addition ( C/O = 0.79) in sample A, as compared to graphs for samples B and C at carbon addition levels of 0.94 and 1.08, respectively.

**Table 4: Reaction times (minutes)**

| Sample Name | Time to first CO formation | Time to hot zone position | Total reaction time | C/O | Aim %Mn recovery | *Furnace Temperature (°C) |
|---|---|---|---|---|---|---|
| A | 23 | 53 | 93 | 0.79 | 70 | 1500 |
| B | 22 | 40 | 111 | 0.94 | 85 | 1500 |
| C | 20 | 38 | 107 | 1.08 | 100 | 1500 |
| D | 19 | 36 | 94 | 0.94 | 85 | 1450 |
| E | 20 | 37 | 74 | 0.94 | 85 | 1550 |
| F | 21 | 28 | 28 | 0.94 | 85 | 1550 |
| G | 22 | 40 | 40 | 0.94 | 85 | 1550 |

*Furnace hot zone temperature

**Table 5: Bulk alloy analyses (mass%)**

| Sample Name | %Fe | %Mn | %C | Total | C/O | Aim %Mn recovery | *Furnace Temperature (°C) |
|---|---|---|---|---|---|---|---|
| A | 12.0 | 79.9 | 7.76 | 99.7 | 0.79 | 70 | 1500 |
| B | 12.0 | 76.5 | 8.73 | 97.3 | 0.94 | 85 | 1500 |
| C | 10.5 | 80.3 | 8.04 | 98.8 | 1.08 | 100 | 1500 |
| D | 13.1 | 73.1 | 7.99 | 94.2 | 0.94 | 85 | 1450 |
| E | 11.7 | 77.3 | 8.22 | 97.5 | 0.94 | 85 | 1550 |
| F | Insufficient coalesced alloy | | | | 0.94 | 85 | 1550 |
| G | Insufficient coalesced alloy | | | | 0.94 | 85 | 1550 |

**Figure 3: Photographs of polished sections**
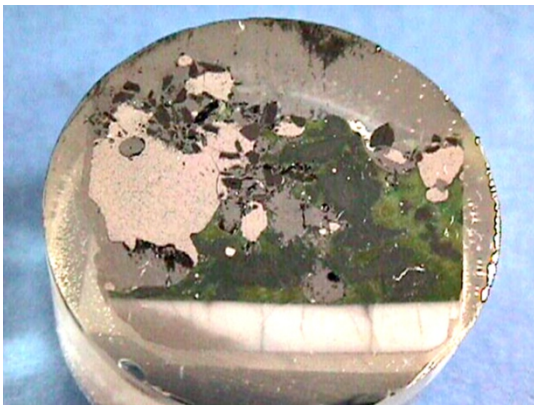
*Sample A*
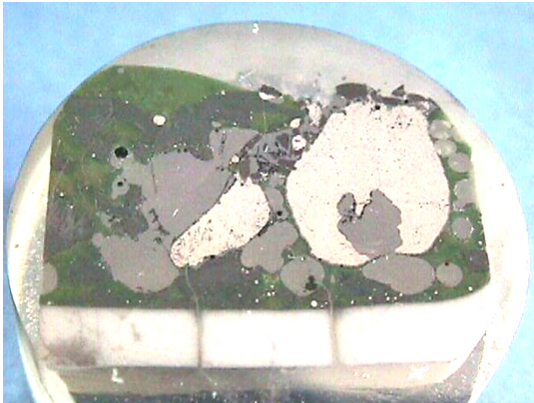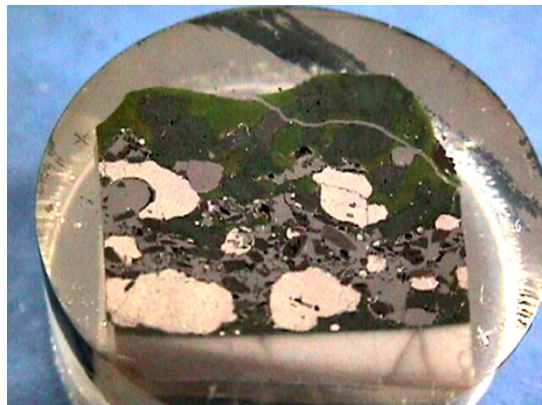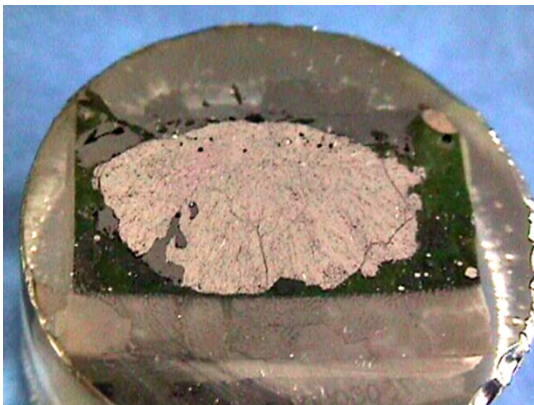
*Sample B*



Sample C

Sample D



Sample E

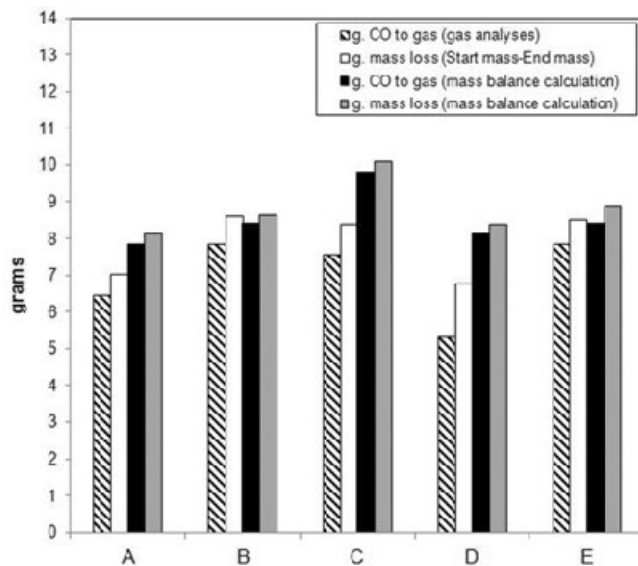Sample G

## 3.2. Mass balance

Mass loss values from the product gas analyses and mass loss measurements (sample mass before reaction minus sample mass after reaction) were compared to the mass loss values as calculated from a mass balance. Mass balance calculations were based on the following assumptions: %Fe recovery to alloy is 100%, only CO gas formed from reduction of oxygen from iron and manganese oxides, the level of %Mn recovery to alloy was set to the level required to attain %Mn in the alloy equal to the normalised bulk alloy analysis contained in Table 5. The calculated alloy analyses, alloy masses and percentage manganese recovery to alloy are summarised in Table 6. The comparative values are summarised in Figure 4. The calculated mass loss differed by a maximum of 1.7 grams from the measured mass loss for sample C. For samples A to E, the mass balance calculation indicated insufficient quantities of carbon available to attain the alloy carbon analysis in Table 5. These values of mass carbon shortage are summarised in Table 6.

**Figure 4: Mass loss values: measured vs. mass balance calculated**



**Table 6: Mass balance calculated values**

| Sample Name | %Mn | %Fe | %C | g. C deficit[1] | mol CO measured | mol CO calculated | %Mn recovery | g. Alloy calculated |
|---|---|---|---|---|---|---|---|---|
| A | 80.2 | 15.8 | 3.99 | 0.61 | 0.28 | 0.23 | 63 | 16.0 |
| B | 78.6 | 14.5 | 6.89 | 0.36 | 0.30 | 0.28 | 67 | 17.5 |
| C | 81.2 | 12.5 | 6.34 | 0.37 | 0.35 | 0.27 | 81 | 20.4 |
| D | 77.6 | 14.8 | 7.60 | 0.15 | 0.29 | 0.19 | 65 | 17.2 |
| E | 79.6 | 14.2 | 6.19 | 0.40 | 0.30 | 0.28 | 69 | 17.9 |

[1]mass of carbon required to increase %C in to normalised analysed bulk alloy %C shown in Table 5

## 3.3.    Phase chemistry

Phase chemical analyses of the product polished sections were done to further investigate the reaction products. Phase chemistry in the polished sections were analysed by SEM (Scanning electron microscopy) using wavelength-dispersive X-ray spectrometry (WDX). Equilibrium phase chemistry calculations were made with FactSage 6.4 thermochemical calculation software, using the FToxid and SGTE databases (Bale et al., 2002).

Because the experimental measurements indicate that molten phase development with heating time is an important aspect in manganese reduction from the ore, changes in slag phase chemistry was investigated in more detail. In Figure 5 changes in slag phase basicity and %MnO, measured by SEM, is plotted for each sample reacted.

Only sample F, reacted for 28 minutes, displayed a changing trend in analyses, from B3 basicity of 0.7 to 1.3 at associated percentage manganosite of 47%MnO to 26%MnO, as compared to the rest of the samples which all displayed analyses close to the target bulk slag phase chemistry of B3=1.34 and %MnO=25. Therefore, the slag phase analyses for sample F, contained in Table a in the Appendix, were compared to the equilibrium liquidus slag chemistry calculated within the system of $MgO-CaO-SiO_2-MnO$ using FactSage 6.4 thermochemical software, plotted in Figures 6 and 7.

The analyses data plots in Figures 6 and 7 indicate that slag phase liquidus temperatures were below 1400°C, even though bulk ore chemistry (illustrated as reduction path line plots for Mamatwan ore in Figure 6 and 7) is of much higher melting point. This disparity in melting point is possible because of formation of monoxide solid solution phase consisting of MnO and some MgO (SEM analyses contained in Appendix, Table b), thus resulting in lower levels of MnO and MgO in the main oxide phase, enabling its melting to slag at relatively low temperatures. This is an important aspect in manganese ore reduction because MnO is not reduced by CO alone, but close proximity of C to the reduction interface is critically important to maintain sufficiently reducing conditions to drive MnO reduction (Kleyenstuber, 1979). Slag formation allows for improved contact between the carbon particle surfaces and oxide phases (reduction sites). In addition slag flow allows for renewal of contact interfaces, as compared to stagnant solid particles of ore and carbon.

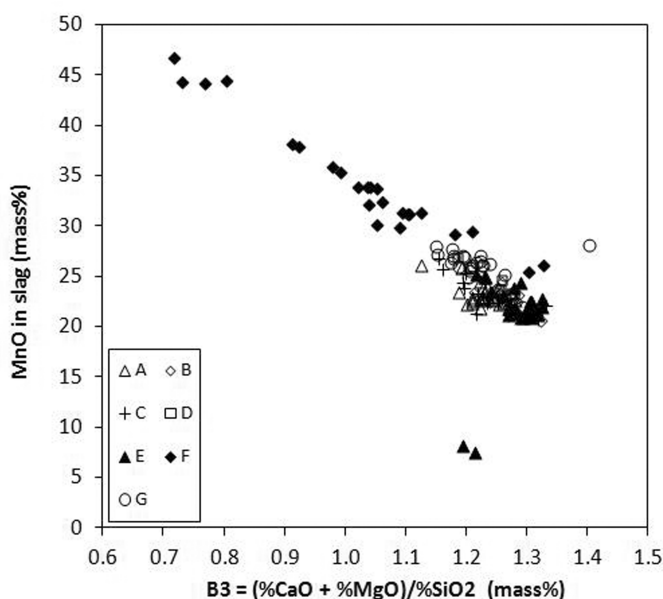**Figure 5: Slag phase B3 vs. mass% MnO in slag**

**Figure 6: Liquidus projection in the 3%MgO-SiO₂-CaO-MgO system (numbers are sample F analyses shown in appendix, Table a)**
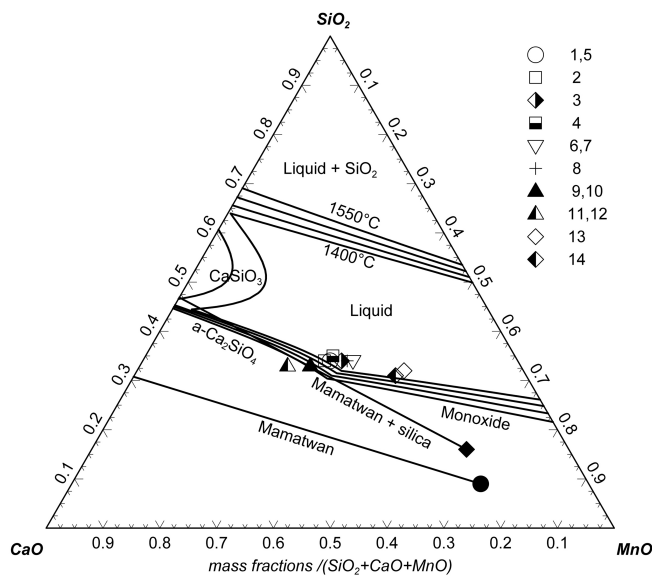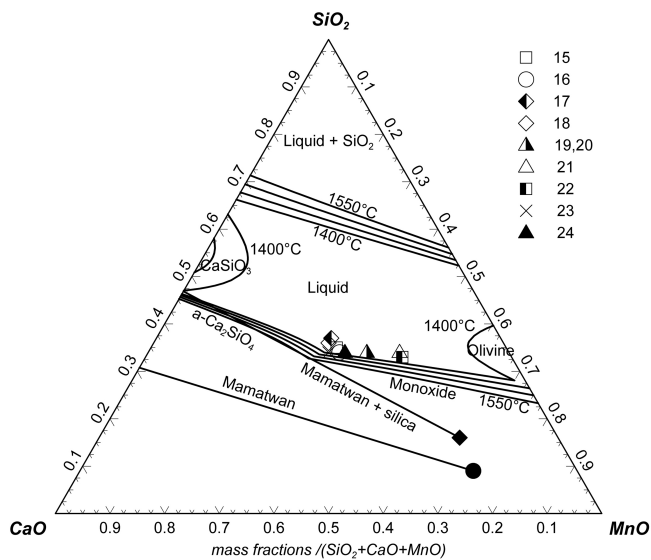


**Figure 7: Liquidus projection in the 6%MgO-SiO₂-CaO-MgO system (numbers are sample F analyses shown in appendix, Table a)**



The alloy SEM analyses for all the polished sections are plotted in Figure 8. It is seen that there is a concentration of analyses at high levels of %Mn (80-90%) and %C (6-9%) for samples A-E and G, whilst sample F alloy analyses contain maximum 63% Mn at 6% C. Figures 9 and 10 display these cumulative analyses trends for samples A-E and G versus that for sample F. Therefore, similarly to the slag phase analyses in sample F,

alloy phase analyses in this sample displays a broad range of phase chemistry in a development trajectory as compared to that in the rest of the samples, which were concentrated at end-point reaction alloy analyses levels.

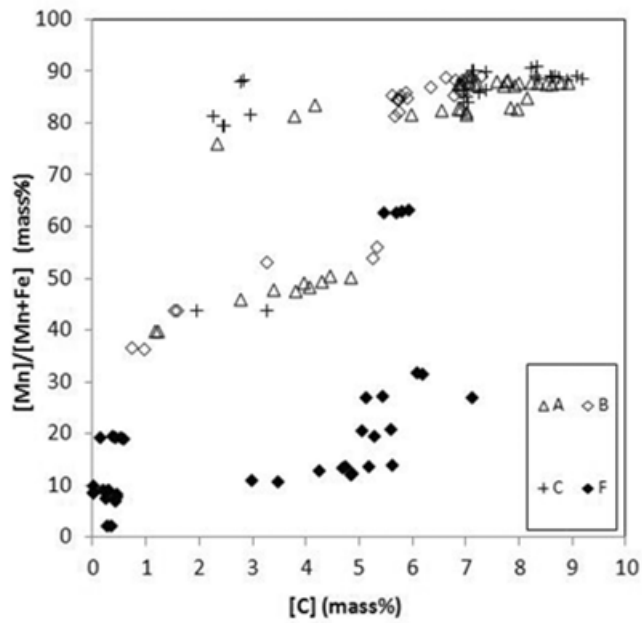**Figure 8(a): Alloy phase chemistry (SEM) in samples A-C and F**
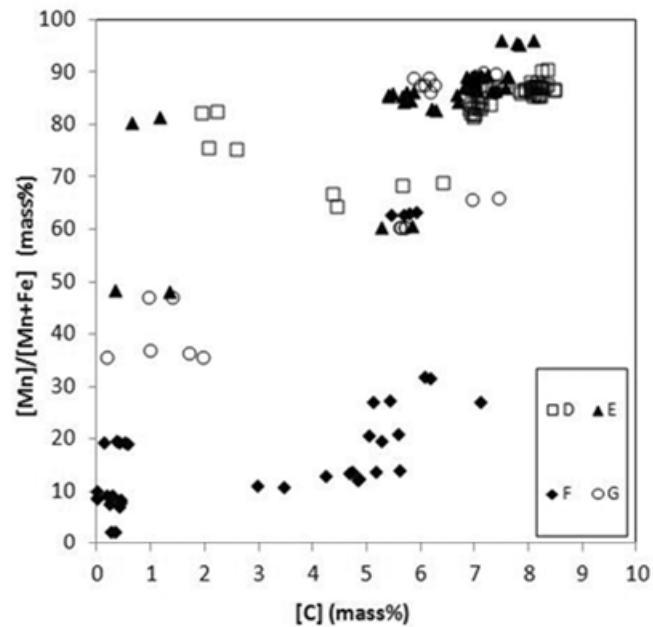


**Figure 8(b): Alloy phase chemistry (SEM) in samples D-G**

**Figure 9: Cumulative alloy phase analyses: %Mn/(%Mn+%Fe) in alloy (SEM)**
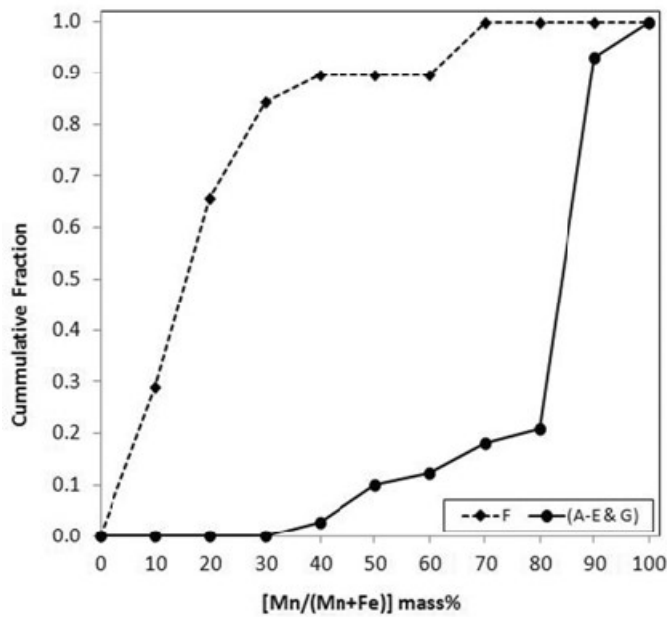


**Figure 10: Cumulative alloy phase analyses: %Carbon in alloy (SEM)**
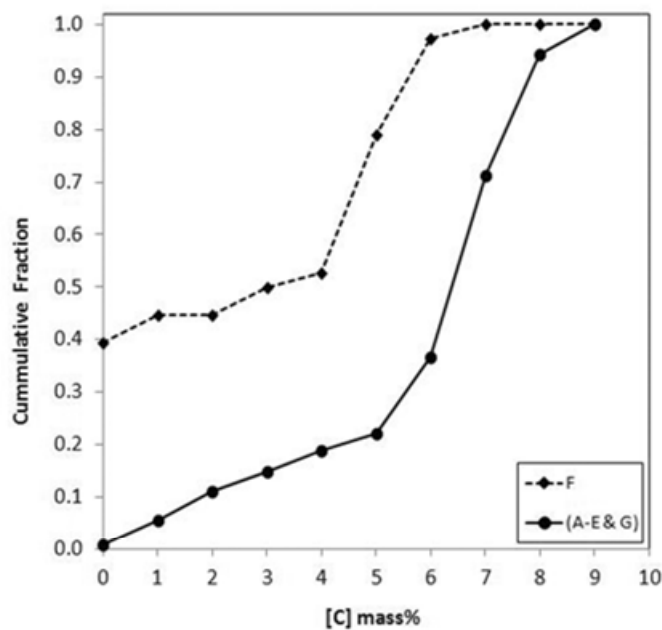


Equilibrium alloy liquidus temperatures were calculated in FactSage 6.4 thermochemical software for sample F analyses, for comparison to the slag liquidus temperatures in Figures 6 and 7. The diagrams in Figure 11 (a-c) illustrate that the alloy liquidus temperatures display a u-shaped trend with increased manganese and carbon content in the alloy beads. The result is that the alloy liquidus temperature is initially high as the alloy beads formed are low in %Mn and %C. Then as reduction proceeds and more manganese is reduced to alloy and carbon dissolved into the alloy the result is a decrease in alloy liquidus temperatures. Comparison of slag phase liquidus temperatures in Figures 6 and 7 to alloy phase liquidus temperatures in Figure 11 indicates that

the slag phase liquidus temperatures are mostly close to 1400°C, and alloy phase liquidus temperatures varied from 1500°C to 1150°C, with most results below 1300°C. Formation of low melting point slag phases will in part contribute to the absence of significant alloy carbon refinement according to reaction (1) because the liquid slag phase closed off original pores in the pre-reduced ore particles, and prevent $CO_2$ access to the alloy phases. In high carbon ferromanganese production in the SAF the bulk of manganese units in the feed mixture is made as lump ore so that slag formation is set by ore chemistry with little possibility of manipulating oxide melting behaviour in the feed mixture (Coetsee et al., 2014). Only when agglomerates such as pellets or sinters are used, may the oxide chemistry be manipulated to limit slag formation to facilitate gas access to alloy beads for reaction (1) to possibly drive carbon refinement.

**Figure 11(a): Alloy phase diagram: 0%Carbon (numbers are sample F analyses shown in appendix, Table c)**
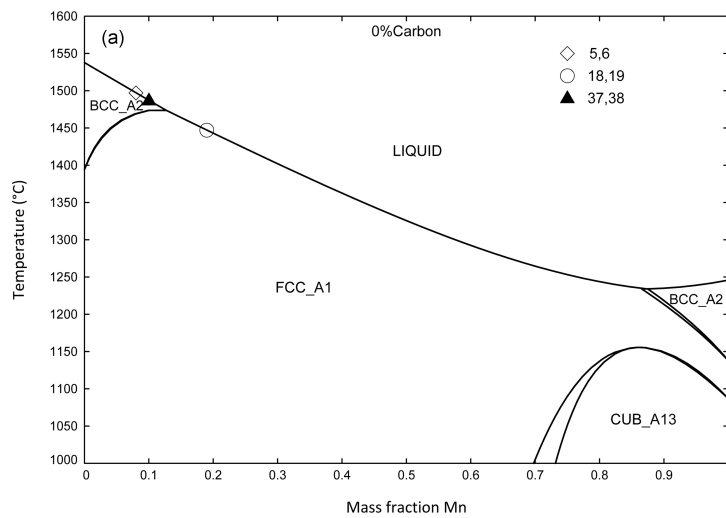


**Figure 11(b): Alloy phase diagram: 3%Carbon (numbers are sample F analyses shown in appendix, Table c)**
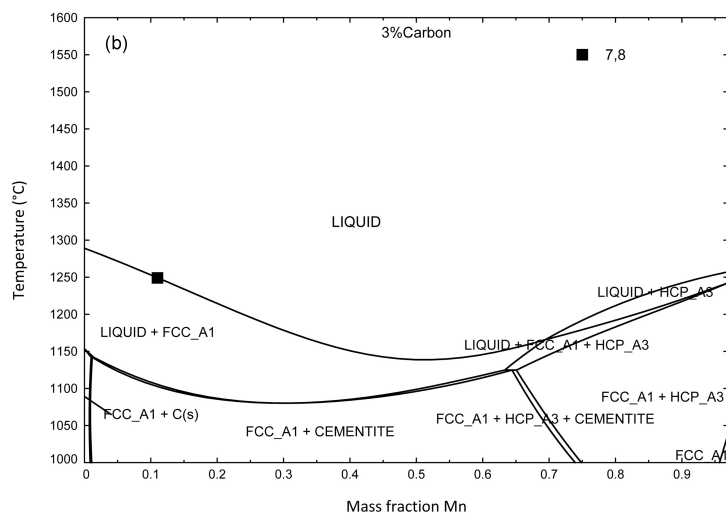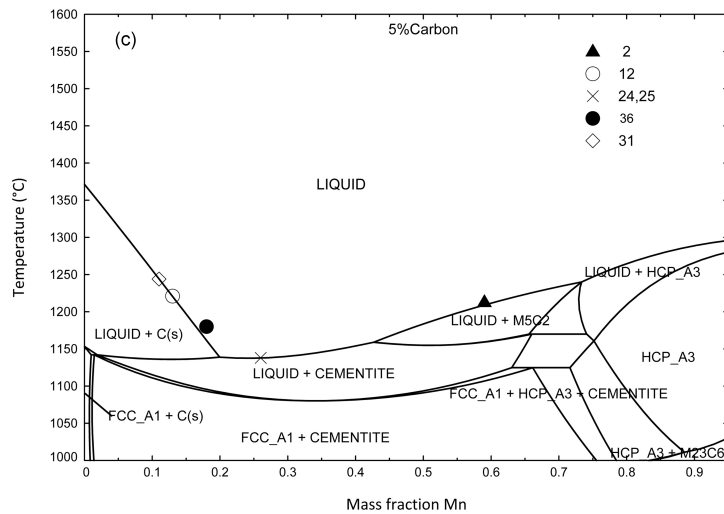
**Figure 11(c): Alloy phase diagram: 5%Carbon (numbers are sample F analyses shown in appendix, Table c)**



## 3.4. Pilot plant furnace alloy composition

High carbon ferromanganese alloy tapped from the AlloyStream pilot plant furnace contained in the order of 6.5%C at a tapping temperature of 1550°C. This unsaturated level of carbon was in part made possible because the hearth refractories were made of MgO, as compared to carbon refractories used is SAF furnaces. The alloy bath consisted of a reservoir mass of 20 tonnes. However, given the high level of carbon in the feed mixture as compared to the laboratory results discussed above, formation of carbon unsaturated alloy is unexpected. Throughout the pilot plant campaign spanning four months, heap samples were collected for characterisation as reported in detail (Coetsee et al., 2015). In addition, alloy beads (>1 mm diameter) were collected from the heap material and analysed by ICP-OES and LECO. Table 7 illustrates selected heap alloy bead analyses and the associated metal tap alloy analyses from the 7 weeks period in which an ore mixture of 90% Mamatwan ore and 10% Wessels ore was used with silica flux and medium volatile thermal coal from Exxaro's Leeuwpan colliery.

It is seen that the two sets of analyses are similar, indicating that little or no refining of carbon or addition of manganese took place as the initially formed alloy beads moved down the solid heap to the metal bath. For comparison to laboratory experimental mixtures in Table 4, the level of carbon addition in the feed mixture is expressed as moles of fixed carbon in coal to moles of reducible oxygen in the ore mixture (reducible oxygen is the moles of oxygen associated with manganese and iron oxides in the ore expressed as $Mn_2O_3$ and $Fe_2O_3$). Part of the coal fixed carbon is burnt in the furnace combustion zone, therefore excess carbon beyond FC/O=1.0 was required in the feed mixture. The level of alloy carbon undersaturation is illustrated in Figure 12 by comparison of the alloy carbon content values from Table 7 to tapped alloy carbon saturation levels at 1550°C.

**Table 7: Heap alloy bead and tapped alloy analyses**

| Sample Number | %C | %Mn | %Fe | %Si | %P | %S | Total | [3]FC/O in feed mixture |
|---|---|---|---|---|---|---|---|---|
| [1]T1 | 6.70 | 78.6 | 14.1 | 0.30 | 0.07 | 0.007 | 99.8 | 1.4 |
| [2]H1 | 6.57 | 73.0 | 19.0 | 0.18 | 0.10 | 0.019 | 98.9 | |
| T2 | 6.58 | 78.9 | 14.2 | 0.21 | 0.08 | 0.003 | 100.0 | 1.4 |
| H2 | 6.88 | 76.9 | 15.2 | 0.19 | 0.08 | 0.008 | 99.3 | |
| T3 | 6.75 | 77.8 | 14.8 | 0.36 | 0.10 | 0.007 | 99.8 | 1.5 |
| H3 | 6.67 | 76.7 | 15.6 | 0.03 | 0.11 | 0.004 | 99.1 | |
| T4 | 6.72 | 79.6 | 14.5 | 0.01 | 0.10 | 0.003 | 100.9 | 1.5 |
| H4 | 6.63 | 79.5 | 11.9 | 0.37 | 0.11 | 0.016 | 98.5 | |
| T5 | 6.73 | 78.6 | 14.8 | 0.09 | 0.12 | 0.004 | 100.3 | 1.6 |
| H5 | 6.83 | 77.5 | 14.1 | 0.20 | 0.15 | 0.010 | 98.8 | |
| T6 | 6.88 | 79.0 | 14.4 | 0.07 | 0.11 | 0.004 | 100.5 | 1.5 |
| H7 | 7.06 | 79.5 | 13.6 | 0.12 | 0.12 | 0.017 | 100.4 | |
| T7 | 6.69 | 78.9 | 14.4 | <0.01 | 0.12 | 0.003 | 100.1 | 1.5 |
| H7 | 6.76 | 73.8 | 19.0 | 0.15 | 0.13 | 0.012 | 99.9 | |
| T8 | 6.79 | 79.5 | 14.5 | <0.01 | 0.11 | 0.003 | 100.9 | 1.5 |
| H8 | 6.69 | 73.0 | 18.8 | 0.15 | 0.17 | 0.010 | 98.8 | |
| T9 | 6.64 | 79.1 | 14.4 | 0.04 | 0.13 | 0.003 | 100.3 | 1.6 |
| H9 | 7.07 | 83.8 | 8.4 | 0.19 | 0.09 | 0.009 | 99.6 | |
| T10 | 6.78 | 78.1 | 14.6 | 0.04 | 0.12 | 0.003 | 99.6 | 1.6 |
| H10 | 6.86 | 79.3 | 13.3 | 0.19 | 0.13 | 0.008 | 99.8 | |
| T11 | 6.58 | 78.1 | 14.3 | 0.13 | 0.12 | 0.006 | 99.2 | 1.6 |
| H11 | 6.33 | 72.2 | 19.9 | 0.14 | 0.16 | 0.010 | 98.7 | |
| T12 | 5.77 | 78.0 | 15.4 | 0.02 | 0.15 | 0.001 | 99.3 | 1.6 |
| H2 | 6.51 | 73.7 | 17.8 | 0.38 | 0.22 | 0.013 | 98.6 | |
| T13 | 6.12 | 78.1 | 15.3 | 0.07 | 0.18 | 0.001 | 99.8 | 1.6 |
| H13 | 6.75 | 77.1 | 15.5 | 0.18 | 0.17 | 0.009 | 99.7 | |

[1] Tapped alloy = T; [2] Heap alloy = H; [3] Fixed carbon to reducible oxygen

Figure 13 indicates the liquidus temperatures (the temperature of initial solid phase formation in the form of either graphite or $M_7C_3$) of the alloy compositions in Table 7. These values indicate that the temperature of formation of the initial alloy is in the order of 1300°C to 1400°C, significantly lower than the alloy bath temperature of 1550°C. In addition, the partial pressure of CO at the top of the heap is unlikely to be at 100% given the material feed mixture contained Mamatwan ore which calcined, and coal which devolatilised at the heap surface. Levels of CO below 100% at the heap surface, unlike the high CO levels in the laboratory experiments reported here and in the coke bed of the SAF, will facilitate lower levels of carbon in primary alloy formation. In this way, at lower levels of reaction temperatures and lower %CO at the top of the heap in the AlloyStream process, with no or little subsequent carbon addition to the primary alloy, an undersaturated carbon alloy product was tapped from the AlloyStream furnace.

**Figure 12: Alloy %C in heap alloy beads vs. tapped alloy vs. tapped alloy saturation at 1550°C**
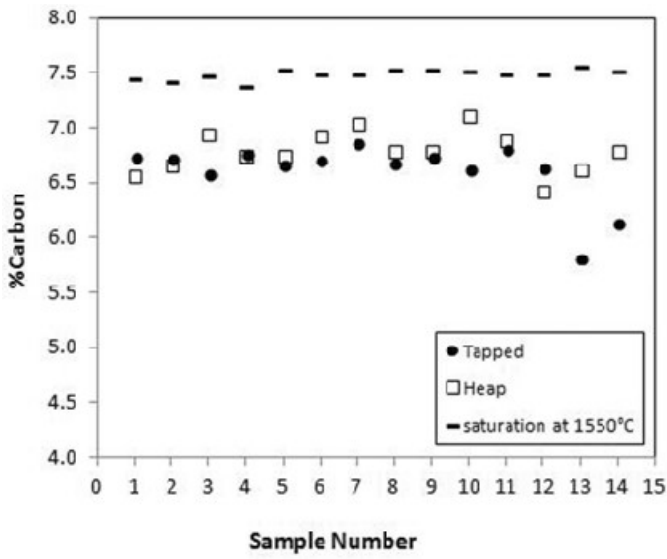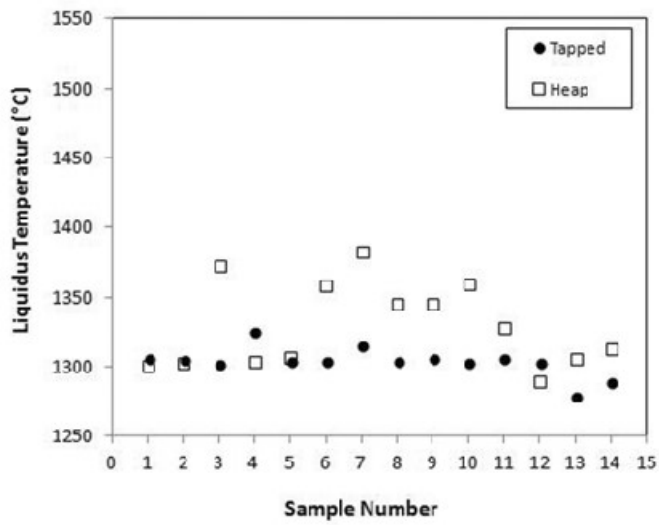


**Figure 13: Liquidus temperatures calculated for heap alloy beads and tapped alloy compositions**

## 4. Conclusions

- The main objective of this research was to test the feasibility of producing medium carbon ferromanganese in the carbothermic reduction of Mamatwan ore. The results confirm that medium carbon ferromanganese was not formed as the endpoint alloy product when carbon reductant was used, even when carbon reductant addition levels were well below stoichiometry (C/O = 1.0). However, a range of alloy carbon content levels was measured in uncoalesced alloy areas at 0%C to 9%C, for the feed mixture carbon addition levels tested (C/O=0.79, 0.94 and 1.08).

- The effect of increased temperature from 1450°C to 1550°C on reduction rate was dominant. The effect of carbon addition was only observed at the lower level of carbon addition of C/O of 0.79, as compared to carbon additions at C/O of 0.94 and 1.08, respectively.

- Results from partially reacted samples containing high basicity Mamatwan ore confirmed the acidic phase chemistry of the glass phase formed prior to coalescence of oxide phases into a bulk slag, at B3=0.7-1.3. (Figure 5); and that the bulk of reduction reactions occur below 1450°C with CO as the main gaseous product. Thus, heating of the sample mixture to higher temperatures was only required to attain slag-metal separation.

- Formation of low melting point slag phases may explain the absence of significant alloy carbon refinement by $CO_2$ gas because liquid slag phase closed off the original pores in the pre-reduced ore to block gas access to the alloy phases contained within pre-reduced ore particles.

- Although the endpoint alloy products in the laboratory tests were high carbon ferromanganese, alloy tapped at 1550°C from the AlloyStream pilot plant was not carbon saturated (containing 6.5%C). This lower level carbon ferromanganese product was made possible because of primary alloy bead formation at 1300°C to 1400°C and/or less than 100% CO gas composition formed at the top of the heap.

## 5. Appendix

**Table a: Slag phase analyses (SEM) in Sample F**

| Number | %MgO | %Al$_2$O$_3$ | %FeO | %MnO | %CaO | SiO$_2$ | Total | *B2 | *B3 |
|--------|------|------|------|------|------|------|-------|-----|-----|
| 1 | 3.85 | 0 | 0.30 | 30.16 | 31.06 | 31.59 | 97.0 | 1.0 | 1.1 |
| 2 | 3.56 | 0 | 0.62 | 30.15 | 31.28 | 31.57 | 97.2 | 1.0 | 1.1 |
| 3 | 5.00 | 0.10 | 0.43 | 31.58 | 28.88 | 31.91 | 97.9 | 0.9 | 1.1 |
| 4 | 5.09 | 0.19 | 0.21 | 30.20 | 29.83 | 31.03 | 96.5 | 1.0 | 1.1 |
| 5 | 4.27 | 0.08 | 0.14 | 34.82 | 26.51 | 31.42 | 97.2 | 0.8 | 1.0 |
| 6 | 1.57 | 0.11 | 0.02 | 45.64 | 20.12 | 30.25 | 97.7 | 0.7 | 0.7 |
| 7 | 1.75 | 1.66 | 0.13 | 42.32 | 21.07 | 28.35 | 95.3 | 0.7 | 0.8 |
| 8 | 4.23 | 0 | 0.01 | 32.68 | 28.38 | 31.31 | 96.6 | 0.9 | 1.0 |
| 9 | 5.32 | 0 | 0.32 | 36.41 | 23.29 | 30.99 | 96.3 | 0.8 | 0.9 |
| 10 | 4.62 | 0 | 0.40 | 42.94 | 18.21 | 31.21 | 97.4 | 0.6 | 0.7 |
| 11 | 4.73 | 0.07 | 0.19 | 42.51 | 18.53 | 30.26 | 96.3 | 0.6 | 0.8 |
| 12 | 2.88 | 0 | 0 | 28.61 | 34.70 | 31.03 | 97.2 | 1.1 | 1.2 |
| 13 | 2.87 | 0.04 | 0.37 | 28.64 | 34.76 | 31.82 | 98.5 | 1.1 | 1.2 |
| 14 | 2.36 | 0 | 0.37 | 25.23 | 38.47 | 30.76 | 97.2 | 1.3 | 1.3 |
| 15 | 4.12 | 0.12 | 0.59 | 33.53 | 26.29 | 30.64 | 95.3 | 0.9 | 1.0 |
| 16 | 4.47 | 0 | 0.38 | 32.82 | 28.18 | 31.45 | 97.3 | 0.9 | 1.0 |
| 17 | 4.20 | 0.10 | 0.14 | 32.81 | 28.06 | 31.55 | 96.9 | 0.9 | 1.0 |
| 18 | 4.43 | 0 | 0 | 32.45 | 28.31 | 31.10 | 96.3 | 0.9 | 1.1 |
| 19 | 4.41 | 0 | 0.11 | 31.79 | 29.76 | 32.85 | 98.9 | 0.9 | 1.0 |
| 20 | 4.29 | 0.31 | 0.23 | 30.22 | 30.18 | 31.48 | 96.7 | 1.0 | 1.1 |
| 21 | 6.41 | 0.03 | 2.53 | 28.60 | 27.68 | 32.38 | 97.6 | 0.9 | 1.1 |
| 22 | 6.77 | 0 | 1.29 | 28.49 | 28.19 | 32.06 | 96.8 | 0.9 | 1.1 |
| 23 | 4.67 | 0.04 | 0.34 | 37.20 | 24.08 | 31.45 | 97.8 | 0.8 | 0.9 |
| 24 | 2.26 | 0.18 | 0.90 | 25.06 | 39.27 | 31.88 | 99.6 | 1.2 | 1.3 |

**6.** *B2=(%CaO/%SiO$_2$); B3=(%CaO +%MgO)/%SiO$_2$

**Table b: Monoxide phase analyses (SEM) in Sample F**

| Number | %MgO | %Al$_2$O$_3$ | %FeO | %MnO | %CaO | %SiO$_2$ | Total |
|--------|------|------|------|------|------|------|-------|
| 1 | 3.98 | 0.11 | 0.81 | 91.48 | 1.13 | 0.23 | 97.7 |
| 2 | 4.41 | 0.07 | 0.89 | 90.97 | 1.52 | 0.18 | 98.0 |
| 3 | 3.03 | 0.16 | 0.38 | 92.37 | 0.72 | 0.30 | 97.0 |
| 4 | 2.93 | 0.20 | 0.35 | 94.23 | 0.87 | 0.27 | 98.9 |
| 5 | 3.73 | 0.16 | 0.70 | 93.02 | 0.75 | 0.37 | 98.7 |
| 6 | 3.49 | 0.02 | 0.74 | 92.73 | 0.57 | 0.40 | 97.9 |
| 7 | 4.68 | 0.15 | 0.90 | 89.93 | 2.85 | 0.21 | 98.7 |
| 8 | 4.82 | 0.31 | 0.26 | 88.71 | 2.64 | 0.53 | 97.3 |
| 9 | 2.24 | 0.08 | 0.56 | 89.87 | 3.54 | 0.45 | 96.7 |
| 10 | 2.43 | 0.31 | 0.18 | 90.45 | 3.17 | 0.34 | 96.9 |

**Table c: Alloy analyses (SEM) in Sample F**

| Number | %C | %Fe | %Mn | %P | %S | %Si | Total |
|---|---|---|---|---|---|---|---|
| 1 | 6 | 35.8 | 60.3 | 0.02 | 0.01 | 0.01 | 101.9 |
| 2 | 6 | 35.9 | 60.7 | 0.01 | 0.01 | 0.01 | 102.2 |
| 3 | 6 | 35.9 | 61.0 | 0.01 | 0.00 | 0.01 | 102.9 |
| 4 | 6 | 35.7 | 61.3 | 0.01 | 0.00 | 0.03 | 103.2 |
| 5 | 0 | 93.8 | 7.9 | 0.05 | 0.01 | 0.01 | 102.1 |
| 6 | 0 | 94.0 | 7.9 | 0.06 | 0.01 | 0.00 | 102.4 |
| 7 | 3 | 88.6 | 11.0 | 0.09 | 0.05 | 0.03 | 102.8 |
| 8 | 4 | 88.5 | 10.8 | 0.09 | 0.05 | 0.03 | 103.0 |
| 9 | 0 | 91.9 | 9.3 | 0.02 | 0.01 | 0.01 | 101.5 |
| 10 | 0 | 92.6 | 9.2 | 0.03 | 0.00 | 0.01 | 102.1 |
| 11 | 4 | 84.8 | 12.7 | 0.06 | 0.01 | 0.0 | 101.9 |
| 12 | 5 | 83.9 | 13.4 | 0.01 | 0.00 | 0.00 | 102.6 |
| 13 | 6 | 83.5 | 13.5 | 0.02 | 0.01 | 0.01 | 102.8 |
| 14 | 0 | 92.1 | 8.6 | 0.22 | 0.01 | 0.01 | 101.3 |
| 15 | 0 | 93.1 | 7.2 | 0.14 | 0.01 | 0.01 | 100.9 |
| 16 | 0 | 98.0 | 2.3 | 0.01 | 0.01 | 0.00 | 100.6 |
| 17 | 0 | 98.0 | 2.3 | 0.02 | 0.01 | 0.01 | 100.6 |
| 18 | 0 | 81.7 | 19.8 | 0.08 | 0.00 | 0.38 | 102.3 |
| 19 | 0 | 81.2 | 19.6 | 0.12 | 0.00 | 0.40 | 101.8 |
| 20 | 7 | 70.6 | 26.2 | 0.08 | 0.01 | 0.08 | 104.3 |
| 21 | 0 | 80.2 | 19.3 | 0.35 | 0.01 | 0.94 | 100.9 |
| 22 | 1 | 80.8 | 19.0 | 0.37 | 0.00 | 1.01 | 101.7 |
| 23 | 1 | 80.7 | 19.5 | 0.41 | 0.00 | 0.93 | 102.1 |
| 24 | 6 | 70.4 | 26.6 | 0.01 | 0.01 | 0.03 | 102.7 |
| 25 | 5 | 70.8 | 26.3 | 0.01 | 0.01 | 0.01 | 102.3 |
| 26 | 5 | 83.6 | 13.2 | 0.01 | 0.01 | 0.01 | 101.6 |
| 27 | 5 | 83.0 | 13.3 | 0.01 | 0.00 | 0.00 | 101.1 |
| 28 | 0 | 91.0 | 8.6 | 0.02 | 0.01 | 0.01 | 99.7 |
| 29 | 0 | 91.7 | 8.7 | 0.01 | 0.01 | 0.01 | 100.4 |
| 30 | 5 | 83.6 | 11.9 | 0.01 | 0.00 | 0.01 | 100.4 |
| 31 | 5 | 84.0 | 11.5 | 0.00 | 0.01 | 0.01 | 100.4 |
| 32 | 7 | 68.4 | 31.7 | 0.14 | 0.01 | 0.85 | 107.6 |
| 33 | 7 | 69.5 | 32.5 | 0.13 | 0.01 | 0.80 | 109.5 |
| 34 | 5 | 75.6 | 19.8 | 0.02 | 0.01 | 0.01 | 100.6 |
| 35 | 5 | 70.9 | 18.8 | 1.25 | 0.01 | 0.03 | 96.3 |
| 36 | 5 | 74.4 | 18.0 | 0.29 | 0.01 | 0.07 | 98.0 |
| 37 | 0 | 88.9 | 10.0 | 0.42 | 0.00 | 1.36 | 100.7 |
| 38 | 0 | 89.3 | 9.2 | 0.41 | 0.00 | 1.64 | 100.8 |

# 6. References

Bale, C.W., Chartrand, P., Degterov, S.A., Eriksson, G., 2002, "FactSage thermochemical software and databases." CALPHAD, 26, pp. 189-228.

Coetsee, T., Zietsman, J., Pistorius, P.C., 2014. "Predicted effect of ore composition on slag formation in manganese ore reduction." Mineral Processing and Extractive Metallurgy, 123, pp. 141-147.

Coetsee, T., Reinke, C., Nell, J., Pistorius, P.C., 2015. "Reduction mechanisms in manganese ore reduction." Metallurgical Transactions B, 46B, pp. 2534-2552.

Eric, R.H., Burucu, E., 1992. "The mechanism and kinetics of the carbothermic reduction of Mamatwan manganese ore fines." Minerals Engineering, 5, pp. 795-815.

Fourie, L.J., 2000, "Metal containing compound reduction and melting process." US patent 6146437.

Habashi, F. (ed.), 1997, Handbook of Extractive Metallurgy, vol. 1, p. 435. Weinheim: Wiley-VCH.

Kleyenstuber, A.S.E., 1979, M.Sc. thesis (in Afrikaans: 'n Mineralogiese Ondersoek van Hoë-temperatuur-reduksieprodukte van Mangaanerts vanuit die Mamatwanmyn, Kalaharimangaanveld), Rand Afrikaans University, Johannesburg, South Africa.

Koursaris, A., Kleynstuber, A.S.E., Finn, C.W.P., 1983. "A mineralogical investigation of the reduction of Mamatwan manganese ore with carbon." Spec. Publ. Geol. Soc. S. Afr., 7, pp. 375-382.

Koursaris, A., See, J. B., 1979. "Discussion: Reactions in the production of high-carbon ferromanganese from Mamatwan ore." .J S. Afr. Inst. Min. Metall., 79, pp. 306-309.

Terayama, K., Ikeda, M., 1985. "Study on reduction of MnO with carbon by effluent gas analysis method." Transactions of the Japan Institute of Metals, 26, pp. 108-114.